FISEVIER

Contents lists available at ScienceDirect

Journal of Magnetism and Magnetic Materials

journal homepage: www.elsevier.com/locate/jmmm



Research articles

Homoepitaxial Mn₃Ge films on ultra-thin Fe seed layer with high perpendicular magnetic anisotropy



Yuyi Wei^{a,1}, Mingmin Zhu^{a,b,c,*,1}, Jiawei Wang^{a,d,*}, Krishnamurthy Mahalingam^e, Benson Athey^e, Gregory M. Stephen^f, Mohsen Zaeimbashi^a, Xinjun Wang^a, Yifan He^a, Huaihao Chen^a, Xianfeng Liang^a, Cunzheng Dong^a, Hao-Miao Zhou^b, Ming Liu^c, Don Heiman^f, John G. Jones^e, Michael E. McConney^e, Piyush Shah^e, Michael R. Page^e, Nian X. Sun^{a,c,*}

- ^a Electrical and Computer Engineering Department, Northeastern University, Boston, MA 02115, USA
- b Key Laboratory of Electromagnetic Wave Information Technology and Metrology of Zhejiang Province, College of Information Engineering, China Jiliang University, Hangzhou 310018. China
- ^c Electronic Materials Research Laboratory, Key Laboratory of the Ministry of Education & International Center for Dielectric Research, Xi'an Jiaotong University, Xi'an 710049, China
- ^d College of Science, Zhejiang University of Technology, Hangzhou 310023, China
- ^e Air Force Research Laboratory, Wright-Patterson AFB, OH 45433, USA
- f Department of Physics, Northeastern University, Boston, MA 02115, USA

ARTICLE INFO

Keywords: Manganese-germanium compound Homoepitaxial film Perpendicular magnetic anisotropy Seed layer

ABSTRACT

The essential step for epitaxial growth of tetragonal Mn_3Ge films with high perpendicular magnetic anisotropy (PMA) is to choose suitable substrates with small lattice misfit. The exploration process has involved large efforts on depositing films on single crystalline substrates using buffer layers preferably formed from Cr or Pt, but they lacked a systematically comparative investigation for practical applications. This study investigates the structural, surface and magnetic properties of ultrathin Fe (2 nm) seed layer to induce homoepitaxial Mn_3Ge films on MgO (0 0 1) substrates compared with that of the heteroepitaxial Mn_3Ge films on three typical buffer layers, such as Cr (40 nm), Cr (20 nm)/Pt (10 nm), Fe (2 nm)/Pt (20 nm). Furthermore, a correlation between film strain and film quality has been established, which is critical for spintronics applications. More importantly, we attribute the homoepitaxial growth of Mn_3Ge films on the ultrathin Fe seed layers to the Fe diffusion and formation of Fe-Mn-Ge alloy at the interface, and confirm this supposition with HAADF-STEM characterizations. The Fe-doped Mn_3Ge interlayer can act as the gradual buffer layer, and lead to a high-quality crystal structure and extremely high magnetic squareness ratio of Mn_3Ge films in a large range of thickness (100 \sim 400 nm). This result offers a new concept of high-quality growth of $D0_{22}$ - Mn_3Ge films, which may enhance the prospect for tetragonal Mn_3Ge thin films in superior spintronics applications.

1. Introduction

The coming "big data" age has required a large demand for fast and nonvolatile memory technologies, in which the spin-transfer-torque magnetic random-access memory (STT-MRAM) has been considered as the most promising one to significantly reduce energy consumption in computers compared with the current dynamic RAM [1]. This STT-MRAM using magnetic tunnel junction (MTJ) as a memory element, shows super gigabit (Gbit) capacities and has strict restriction on the

magnetic electrode materials with low STT-switching current (J_{c0}), high thermal stability factor ($\Delta > 60$), and high tunnel magnetoresistance ratio (TMR > 200%) [2–5]. It is clarified that these requirements can be achieved by using perpendicularly magnetized electrodes with low saturation magnetization (M_S), low Gilbert damping constant (α), high uniaxial anisotropy constant (K_u) and high spin polarization (P) [6]. However, conventional magnetic materials with perpendicular magnetic anisotropy (PMA), such as FeCoB thin film sandwich structure [7], ultrathin Fe/oxide heterostructures [8,9], [Co/Pt]_n and [CoFe/Pt]_n

^{*}Corresponding authors at: Key Laboratory of Electromagnetic Wave Information Technology and Metrology of Zhejiang Province, College of Information Engineering, China Jiliang University, Hangzhou 310018, China (Mingmin Zhu). College of Science, Zhejiang University of Technology, Hangzhou 310023, China (Jiawei Wang). Electrical and Computer Engineering Department, Northeastern University, Boston, MA 02115, USA (Nian X. Sun).

E-mail addresses: mzhu@cjlu.edu.cn (M. Zhu), wangjiawei@zjut.edu.cn (J. Wang), nian@ece.neu.edu (N.X. Sun).

¹ Y. Wei and M. Zhu contributed equally to this work.

multilayers [10], cannot meet all of these criteria. Especially these layers must be made sufficiently thin that their interface PMA overcomes the demagnetization energy arisen from magnetic volume. Therefore, these interface PMA would be too weak for an actual device at a critical dimension to overcome thermal fluctuations, and large efforts should be put on the exploration of novel materials with PMA derived from volume magnetocrystalline anisotropy [11].

Recently, Mn-based tetragonal Heusler alloys have been studied as potential electrode materials for MRAM applications, because of its low M_S , low α , and high K_u . Among these alloys, the Mn-Ga system has been intensively investigated both in theoretical and experimental studies, which exhibits the saturation magnetization of $M_S \sim 200-600$ emu/ cm³, the Gilbert damping constant of $\alpha \sim 0.008$ –0.015, the uniaxial anisotropy constant of $K_u \sim 10-23.5 \text{ Merg/cm}^3$, and spin polarization of $P \sim 40-58\%$, showing great potential application in STT-MRAM [12-19]. On the other hand, the tetragonally distorted D0₂₂-Mn₃Ge compound has been predicted to possess a low damping constant of $\alpha \sim 9 \times 10^{-4}$, a high anisotropy constant of $K_{\nu} > 22.9 \, \mathrm{Merg/cm^3}$, and a high spin polarization of $P \sim 77\%$ (dispersion, 100% in the (0 0 1) crystallographic direction), which could lead to an extremely high TMR for use in spintronics [20-22]. However, the experimental works on DO₂₂-Mn₃Ge films have a long way to go. Lately, (0 0 1)-oriented epitaxial D022-Mn3Ge thin film was first reported to show a rather low anisotropy constant K_u value of 9.1 Merg/cm³ on SrTiO₃ substrate [23]. Further studies about high quality films have been carried out with Cr buffer layer on MgO substrates, with precise control of composition and growth temperature the K_u value can be increased as 11.8 Merg/cm³ [21,24]. Moreover, the Cr/Rh buffer layer was also used to epitaxially grow the Mn₃Ge films, which have a K_u of 11.6 Merg/cm³, comparable to that of the film grown on Cr [25]. It is notable that the magnetic property of Mn₃Ge films with different seed layer or substrates do not degrade or enhance monotonously when the lattice mismatching simply becomes larger or smaller [20,26]. For example, the lattice mismatch between Mn₃Ge and Cr is larger than that between Mn₃Ge and SrTiO₃ substrate or Rh layer, but the films grown on Cr buffer layer exhibit better magnetic properties. On the other hand, Pt shows a smaller lattice mismatch with Heusler alloys, which has also been confirmed to be good choices for the epitaxial growth of Mn_xGa films with flat surfaces and high crystalline quality [16], but the study of Mn₃Ge films on Pt seed layer has been rarely reported [27].

In fact, due to the tetragonal lattice distortion, the strong PMA properties only occur in the DO22 phase of Mn3Ge, with the easy axis along the c direction. Therefore, the epitaxial growth of D0₂₂-Mn₃Ge with (0 0 1) orientation is very critical for obtaining strong PMA and can be significantly affected by the buffer layers between Mn₃Ge films and the substrates. A large effort has been involved on epitaxially growing Mn₃Ge films with sub-100 nm thickness on SrTiO₃ (0 0 1) or Cr-buffered MgO (0 0 1) substrates to pursue excellent magnetic properties, such as giant perpendicular anisotropy, ultrahigh coercivity, and large magnetic energy product, to enhance their applications in STT-MRAM. However, rare work has been put attention on the comprehensive investigation on simultaneously obtaining high magnetic performance, good structural quality, and smooth surfaces in Mn₃Ge films over 100 nm that all are essential for practical applications [11,16]. In this work, a systematic study of sputtered Mn₃Ge films on MgO substrates with various buffer layers, including Cr, Cr-buffered Pt, Fe-buffered Pt, and ultra-thin Fe seed layer, has been investigated. The impacts of buffer layers on the crystallization and magnetic anisotropy of DO₂₂-Mn₃Ge films were experimentally studied in detail, as well as the thickness effects of D022-Mn3Ge films. Most importantly, we show that by using an ultrathin Fe seed layer (2 nm) to induce the homoepitaxial growth of Mn₃Ge films, the best crystal structure and extremely high magnetic squareness ratio can be obtained even in the thick film region (100 \sim 400 nm). This study provides new possibilities for the use of high-quality $D0_{22}$ -Mn $_{3}$ Ge films not only in spintronic devices, but also in THz emitter and oscillator [28-30].

2. Experimental

All Mn₃Ge samples were prepared on MgO (0 0 1) single crystal substrates in the magnetron sputtering chamber with a base pressure less than 2 \times 10 $^{-7}$ Torr. Prior to deposition, the MgO substrates were cleaned by sonication in acetone and ethanol, and then thermally flushed in a vacuum at 600 °C for 15 min. The various buffer layers, including Cr (40 nm) single layer, Cr (20 nm)/Pt (10 nm) bilayer, Fe (2 nm)/ Pt(20 nm) bilayer and Fe (2 nm) single layer, were deposited on the MgO substrates by DC sputtering with optimum procedures [21,24]. The Mn₃Ge layers were grown by co-sputtering Mn and Ge target at 500 °C with thickness varying from 100 nm to 400 nm. Finally. 2 nm-thick Pt layers were deposited as cap layers, following by a 30 min post-annealing at 500 °C. X-ray diffraction (XRD, Bruker, D8 DISCO-VER) was used to determine the crystal structure of the Mn₃Ge films. The films morphology was characterized using field emission scanning electron microscopy (FESEM, Zeiss, SUPRA 25). The interfacial microstructure of the film was characterized by high-angle annular dark-field scanning transmission electron microscopy (HAADF-STEM) using a Chemi-STEM™-SuperX (Thermofisher Scientific) electron microscope equipped with an energy-dispersive X-ray spectroscopy (EDX) detector. The magnetic properties were measured using superconducting quantum interference device vibrating sample magnetometer (SQUID-VSM, Quantum Design, PPMS) at 300 K and the applied fields were up to \pm 5 T for both in-plane and out-of-plane measurements.

3. Results and discussion

3.1. X-ray diffraction studies

Fig. 1 shows the X-ray diffraction patterns of the films on the different buffer layers. The appearance of Mn₃Ge (0 0 4) peak indicates that the film is crystallized in the tetragonal D022 phase, which is a signature of PMA characteristics in films. As can be seen in Fig. 1(a), all Mn₃Ge films grown on different buffer layers exhibit clear D0₂₂ (0 0 4) peaks, indicating that Mn₃Ge films on all buffer layers have the D0₂₂ structure and a (0 0 1) preferential orientation along with MgO (0 0 1) substrates. After normalizing the diffraction intensity with MgO substrate (0 0 2) peak, the Mn₃Ge film on the Fe/Pt buffer layer shows the strongest (0 0 4) peak among all samples, indicating that the film is better crystallized comparing to others. Moreover, the Mn₃Ge film on the ultra-thin Fe (2 nm) seed layer also shows excellent crystallinity with strong D0₂₂ (0 0 4) peak. Therefore, to further compare the growth quality of Mn₃Ge films on Fe/Pt buffer layer and ultra-thin Fe seed layer, we carried out the thickness dependences of XRD spectra for the Mn₃Ge films on these two buffer layers as shown in Fig. 1(b) and (c). With increasing the Mn₃Ge film thickness from 100 nm to 400 nm, only (0 0 4) peaks can be observed in the films on the ultra-thin Fe seed layer, but a secondary phase Mn₃Ge (2 0 0) peak rises in the film on Fe/ Pt buffer layer when the film thickness reaches 400 nm. It can be understood that although the Fe-buffered (0 0 1) oriented Pt buffer has the smallest lattice mismatch (2.8%) within various buffer layers, the intrinsically heterogeneous growth will lead to partially disorientation of unit cell when the film thickness reaches the critical value (400 nm). However, ultra-thin Fe layer only works as a seed layer to induce the epitaxial growth of the film above. It provides Fe diffusion into Mn-Ge alloy, thus will lead to the formation of Fe-Mn-Ge alloy which acts as the new gradual buffer layer for homogeneous film growth. The new buffer layer will give rise to a better epitaxial growth intermediary for thick Mn₃Ge film. This explanation can be further confirmed by our STEM results and coincide with the analysis of c-axis lattice constants of the Mn₃Ge films grown on all buffer layers shown in Fig. 1(d). The caxis lattice constants show an increasing trend as the 300 nm-thick Mn₃Ge films grown on Cr, Cr/Pt, and Fe/Pt buffer layers, respectively, implying that the c-axis lattice strain was mainly derived from the lattice mismatch between Mn₃Ge film and buffer layer. The 300 nm-

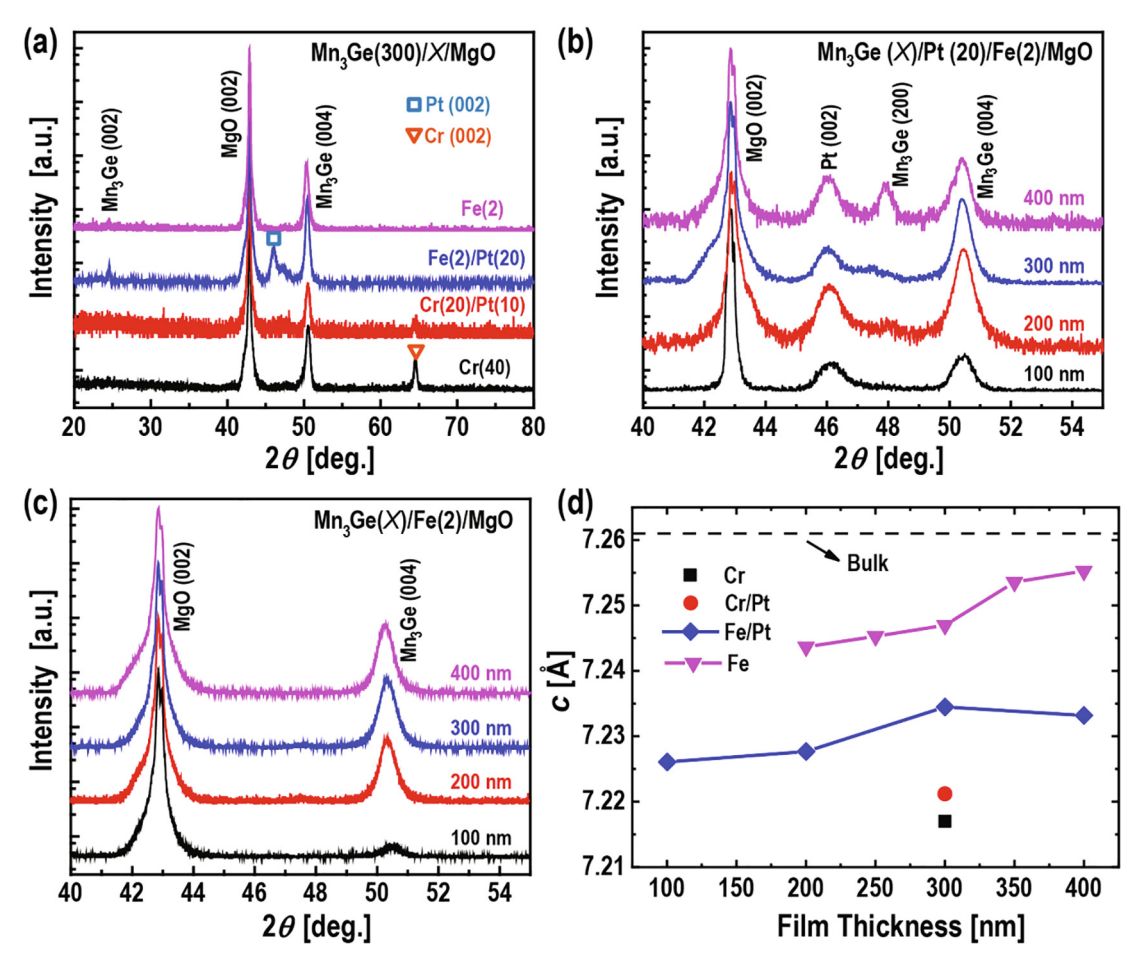


Fig. 1. (a) XRD patterns of Mn_3Ge films on different buffer layers; XRD patterns of Mn_3Ge films with different thicknesses on (b) Fe/Pt buffer layer, and (c) ultra-thin Fe seed layer; (d) Thickness dependence of corresponding c-axis lattice constant of the Mn_3Ge films on the buffer layers, where the dash line shows the c value of bulk Mn_3Ge .

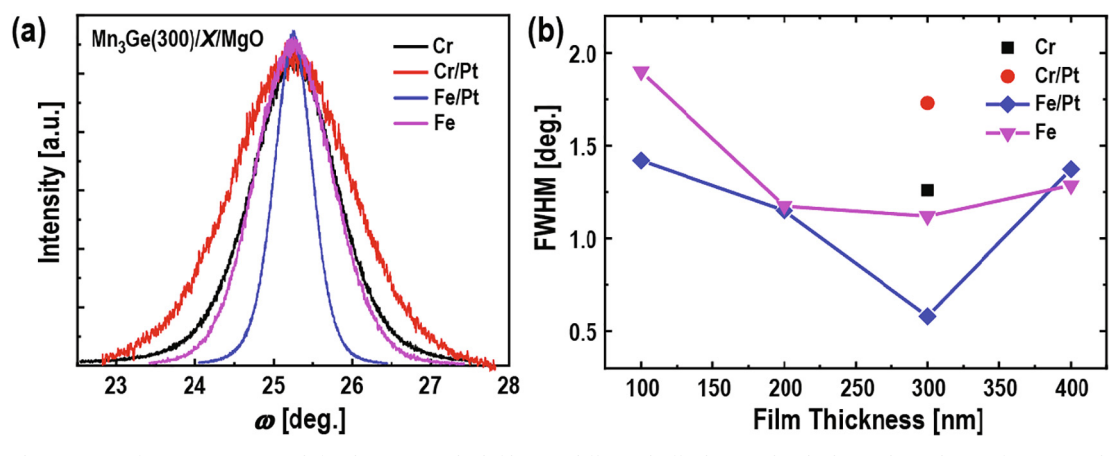


Fig. 2. (a) The rocking curves of (0 0 4) Mn_3Ge peak for the 300 nm-thick films on different buffer layers; (b) Thickness dependence of corresponding FWHM values of the (0 0 4) peaks on different buffer layers.

thick $\rm Mn_3Ge$ film on the ultra-thin Fe seed layer shows the smallest lattice distortion compared with that of the films on other buffer layers. And the lattice constant would approach to the bulk value with increasing film thickness which is a typical character of homogeneous growth. On the other hand, the lattice constant of the film on Fe/Pt layer shows a smaller lattice distortion in the 300 nm-thick $\rm Mn_3Ge$ film, but an increase in the 400 nm-thick film. All these results are consistent with the thickness dependences of XRD spectra shown in Fig. 1(b) and (c), which suggests that the homogeneous growth of $\rm Mn_3Ge$ films on the

ultra-thin Fe seed layer will offer a larger thickness window for deposit epitaxial $\mathrm{Mn_3Ge}$ films with volume PMA properties. This method can have important use and great potential in the next device applications.

X-ray rocking curves of the $Mn_3Ge~(0~0~4)$ peak for the 300 nm-thick films on different buffer layers are presented here to further investigate the crystallization of the films as shown in Fig. 2(a). The (0~0~4) texture is much sharper in the film grown on the Fe/Pt buffer layer which is attributed to the smallest lattice mismatch between Mn_3Ge and Pt. The thickness dependent full-width at half-maximum (FWHM) of the

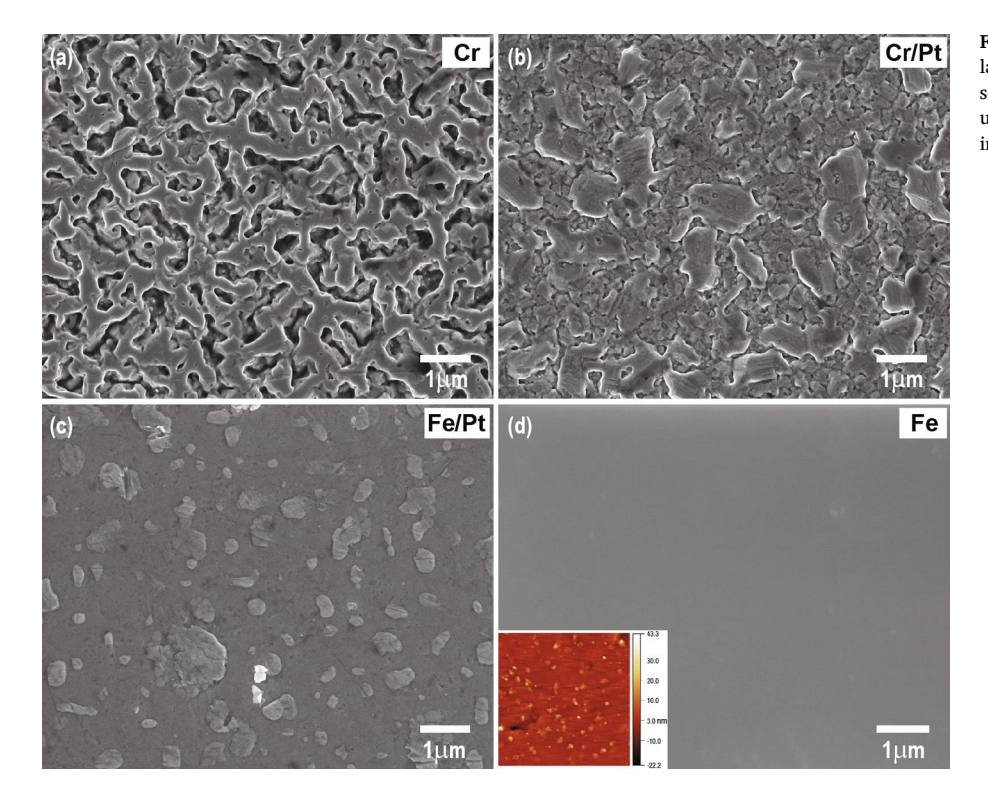


Fig. 3. SEM images of Mn_3Ge films grown on buffer layers of (a) Cr, (b) Cr/Pt, (c) Fe/Pt and (d) ultra-thin seed layer of Fe. AFM image of Mn_3Ge film grown on ultra-thin Fe seed layer with size of 5 μ m \Diamond 5 μ m is inserted in (d).

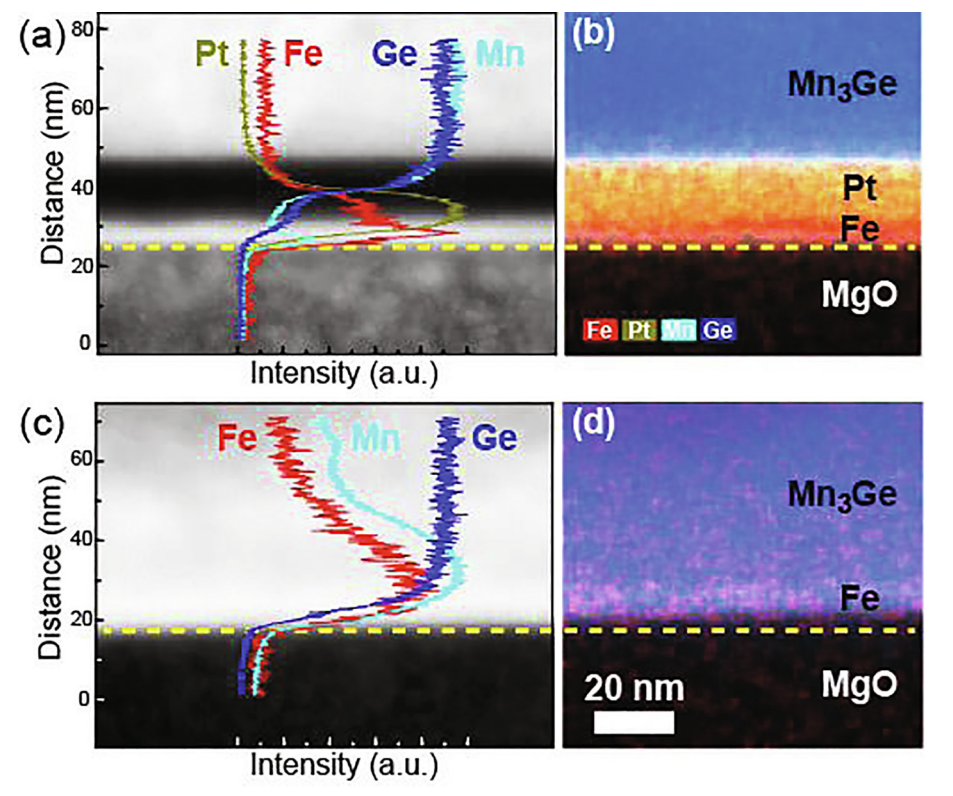


Fig. 4. (a) Cross-section STEM image for the Mn_3Ge film grown on Fe/Pt buffer layer and EDX line profiles of Fe, Pt, Mn, and Ge elements across the film; (b) The corresponding EDX mapping for Mn_3Ge film grown on Fe/Pt buffer layer; (c) Cross-section STEM image for the Mn_3Ge film grown on ultra-thin Fe seed layer and EDX line profiles of Fe, Mn, and Ge elements across the film; (d) The corresponding EDX mapping for Mn_3Ge film grown on ultra-thin Fe seed layer.

rocking curves is collected in Fig. 2(b), which has a varied range from 0.5° to 2° . The smallest FWHM value in the 300 nm-thick Mn_3Ge film on Fe/Pt buffer layer indicates its best crystalline quality, and a broaden FWHM occurred in the 400 nm-thick Mn_3Ge film on Fe/Pt buffer layer may be related to the appearance of the secondary phase, which changes the internal strain of the film. Although the 300 nm-thick Mn_3Ge film on the ultra-thin Fe seed layer has the smallest lattice distortion among the films on all buffer layers as shown in Fig. 1(d), the

Fe diffusion in the Mn_3Ge films may lead to a larger FWHM than that of films on the Fe/Pt buffer layer with finite thicknesses (< 400 nm). But its FWHM is still smaller than those of films on Cr, and Cr/Pt buffer layers. Moreover, the FWHM values of the Mn_3Ge films on the ultrathin Fe seed layer are almost independent of the thickness when the film thickness is larger than 200 nm, indicating that the ultra-thin Fe layer is suitable for a large window of Mn_3Ge films growth.

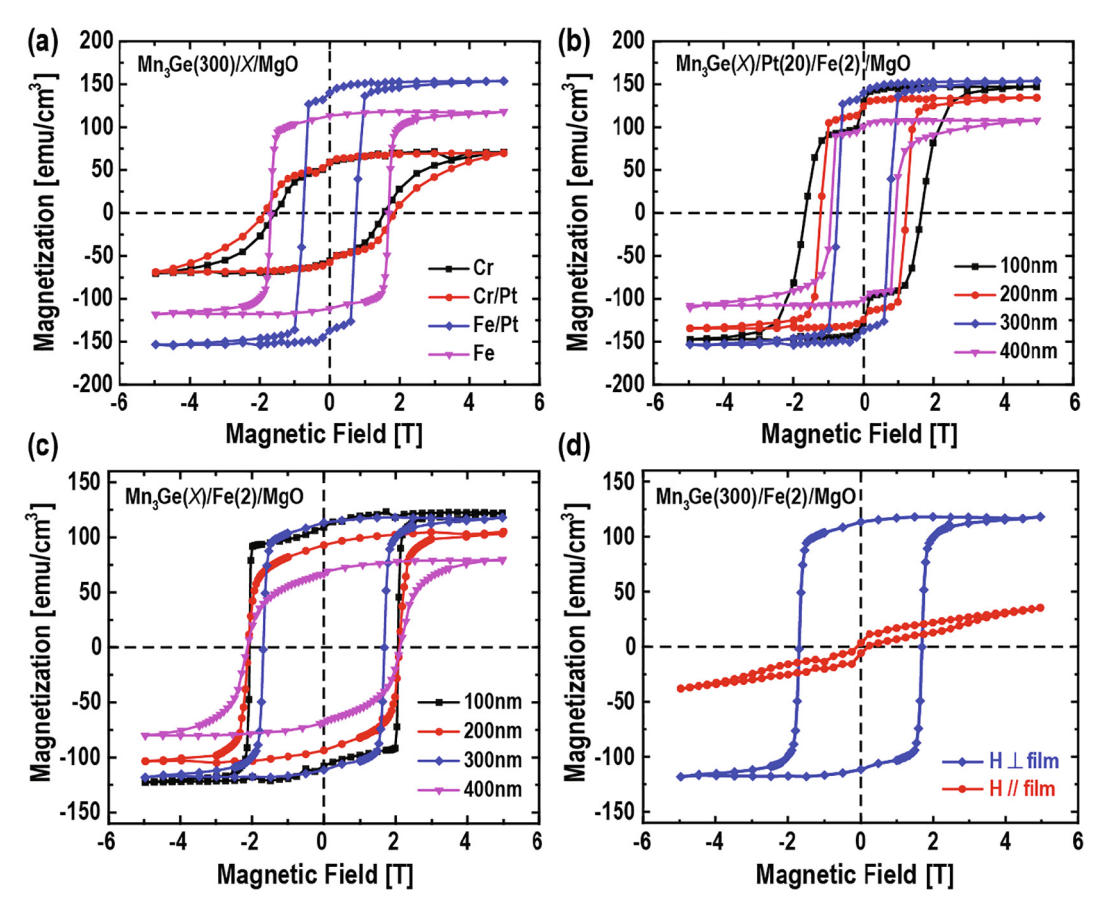


Fig. 5. Magnetization versus field hysteresis loops of Mn_3Ge films grown on (a) different buffer layers with film thickness of 300 nm; (b) Fe/Pt buffer layers with different thicknesses; (c) ultra-thin Fe seed layers with different thicknesses. (d) Typical out-of-plane and in-plane magnetization curves for 300 nm-thickness Mn_3Ge films grown on ultra-thin Fe seed layer.

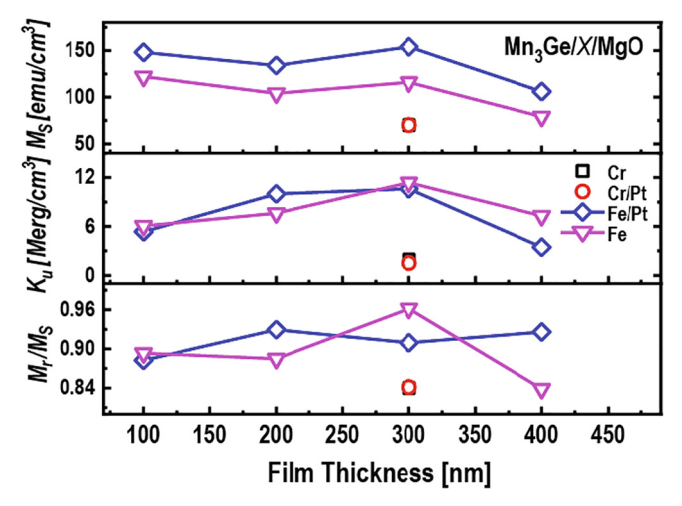


Fig. 6. M_S , K_u values, and M_r/M_S of the Mn₃Ge films as functions of film thickness.

3.2. Surface structure and interface characterizations

Fig. 3 shows the top view images of DO_{22} phase crystallized Mn_3Ge films on different buffer layers. As can be seen, the surfaces of Mn_3Ge films grown on Cr, Cr/Pt, and Fe/Pt buffer layers appeared to be very rough with discontinuous islands, even lots of holes can be observed on the surface of the film deposited on Cr buffer layer due to its largest misfit between Mn_3Ge and Cr. However, a much smoother surface free of pinholes can be observed on the films grown on the ultra-thin Fe seed

layer, which shows a surface roughness Ra of 2.38 nm as derived from the inserted atomic force microscope (AFM) image shown in Fig. 3(d). This smooth surface forming may be resulted from the interface diffusion between ultra-thin Fe and $\rm Mn_3Ge$, which has been confirmed with that the Fe doping can facilitate the surface wetting in Mn-based tetragonal Heusler alloys [31]. Therefore, the smallest surface roughness of $\rm Mn_3Ge$ film on the ultra-thin Fe seed layer may enhance its use to spintronics devices.

Fig. 4 compares the typical interfacial microstructure, as well as relative elemental distribution, of 300 nm-thick Mn₃Ge film grown on Fe/Pt buffer layer and on ultra-thin Fe seed layer. Fig. 4(a) shows the cross-sectional observations for the Mn₃Ge film on Fe/Pt buffer layer by the HAADF-STEM. The layered structure of Mn₃Ge/Pt/Fe/MgO from top to bottom can be clearly identified. EDX line profiles were taken to investigate relative elemental distribution among the individual layers. The compositional distribution of Fe, Pt, Mn and Ge elements across the layers is also plotted in Fig. 4(a), suggesting that the multilayer structure remains chemically sharpened. This can also be confirmed by the corresponding EDX mapping for Mn₃Ge film grown on Fe/Pt buffer layer as shown in Fig. 4(b). Both the microstructure image and element mapping verify the clear interfaces among the Mn₃Ge/Pt/Fe/MgO multilayer. However, as only the ultra-thin Fe seed layer has been used to grow the Mn₃Ge film, no obvious interface can be observed in the cross-section STEM image shown in Fig. 4(c). The EDX line profiles of Fe, Mn, and Ge elements across the film show that the Fe element has spread into Mn₃Ge film and may produce a new alloyed buffer layer like Mn_{3-x}Fe_xGe in the interfacial region. This Fe doping in the epitaxial Mn₃Ge film above makes it reasonable that the c-axis lattice constant of Fe-doped Mn₃Ge film from ultra-thin Fe seed layer should slightly decrease compared to bulk Mn₃Ge. And it will be larger than more

Table 1
Typical magnetic data for Mn₃Ge films grown on different substrates.

Material	Substrate	Seed layer	Lattice mismatch	Film thickness	M _S /emu/cm ³	K _u /Merg/cm ³	H_c/T	Reference
Mn ₃ Ge	SrTiO ₃	N/A	2.3%	100 nm	73	9.1	2.3	[15]
$Mn_{3+x}Ge$	MgO	N/A	10.3%	130 nm	130	10	2	[20]
Mn_3Ge	MgO	Cr	6.9%	130 nm	110	11	1.0	[16]
$Mn_{3+x}Ge$	MgO	Cr	6.9%	130 nm	100	11.8	1.04	[28]
Mn_3Ge	MgO	Cr/Rh	-0.3%	130 nm	115	11.6	1.26	[18]
Mn_3Ge	Si	TaN/IrMn ₃	-1.2%	30 nm	130	5.4	5	[9]
Mn_3Ge	MgO	Fe/Pt	2.8%	300 nm	153	10.6	1	This work
Mn_3Ge	MgO	Fe	5.8%	300 nm	116	11.4	2	This work

A positive (negative) lattice mismatch suggests the Mn₃Ge film is expected to experience tensile (compressive) strain on the corresponding seed layer.

strained $\rm Mn_3Ge$ films on other buffer layers [32,33], which is consistent with the results in Fig. 1(d). Moreover, since the diffusion is not uniform across the whole film, the content of the Fe element in the $\rm Mn_3Ge$ unit cell varies with the distance to the interfacial region. The lattice constants of the $\rm Mn_3Ge$ film around the interfacial region are rather complicated, which will reduce the crystallization of the film and broaden the FWHM as shown in Fig. 2(b). This Fe diffusion phenomenon has also been displayed in its EDX mapping result shown in Fig. 4(d). The different interfacial behavior between $\rm Mn_3Ge$ films grown on Fe/Pt buffer layer and ultra-thin Fe seed layer could lead to different PMA properties, which will be expounded next.

3.3. Magnetic behaviors

Fig. 5 shows the magnetic properties of the films measured at room temperature with all substrate diamagnetic signals subtracted. The typical out-of-plane M-H loops of the 300 nm-thick Mn₃Ge film on different buffer layers are displayed in Fig. 5(a). The magnetization hysteresis loops show clear PMA properties of all films, while the samples on Fe/Pt buffer layer and ultra-thin Fe seed layer have larger M_S (153 and 116 emu/cm³, respectively) and much better squareness (M_r/M_S) compared with the samples on Cr and Cr/Pt buffer layers. Among these loops, the smoothest M-H loop can be observed in the Mn₃Ge film on the ultra-thin Fe seed layer, corresponding to its best crystallization degree and lowest lattice strain as shown in Fig. 1. Another noteworthy item is that a kink is observed in the M-H loops of the samples on Fe/Pt buffer layers, shown more clearly when film thickness decreases as shown in Fig. 5(b). This canted effect is due to the effect of the interface magnetic Fe layer [33], which can be observed in the STEM image. However, the Mn₃Ge films on the ultra-thin Fe seed layer have no such canted magnetic moment as shown in Fig. 5(c), which may be resulted from the Fe diffusion induced homogeneous Fe-doped Mn₃Ge interlayer that has similar PMA characteristics with pure Mn₃Ge thin film [31], and this alloyed behavior can be confirmed with the EDX line profiles. Therefore, the M-H loops of films on ultra-thin Fe seed layers indicate a single-phase behavior that is more desirable. Moreover, the in-plane and out-of-plane M – H loops for the 300 nm-thick sample on the ultra-thin Fe seed layer are displayed in Fig. 5(d). A broad hysteresis with a coercivity of about 3 T can be observed for the perpendicular field curve, while a non-saturating hard axis magnetization can be observed for the in-plane field curve. These typical magnetization hysteresis curves have further confirmed the well PMA property of the film.

The detailed evolution of saturation magnetization M_S , magnetic anisotropy K_u , and squareness M_r/M_S with film thickness varying for the Mn_3Ge films is shown in Fig. 6, where the K_u value is estimated from $K_u = H_{eff} \times M_s/2 + 2\pi M_s^2$ [11]. As can be seen, a maximum K_u value of 11.4 Merg/cm³ is obtained in 300 nm-thick samples on the ultra-thin Fe seed layer, as well as the maximum value with the squareness close to 1, showing the best PMA properties in this sample. The typical magnetic data for Mn_3Ge films grown on different substrates have been compared in Table 1. Comparing to the best reported K_u value of 11.8 Merg/ cm³

in the films with stoichiometric compositions [22], our results show comparable PMA properties in the homoepitaxial Mn_3Ge film on the ultra-thin Fe seed layer. Although the saturation magnetization for the Mn_3Ge films on Fe/Pt and Fe buffer layers in all film thickness range is much larger than that of Mn_3Ge films on Cr and Cr/Pt buffer layers, this may be mainly originated from the ferromagnetic Fe sublattices. The interface Fe diffusion in Mn_3Ge films makes the magnetization of samples on ultra-thin Fe seed layer practically quenched and keep a low-value level among all reported results as shown in Table 1 [31]. Thus, we suggest that the ultra-thin Fe seed layer would be strong candidate for growing thick Mn_3Ge films with high anisotropy and low magnetization being used in spintronics devices.

4. Conclusions

In summary, we have compared the effects of different buffer layers on the epitaxial growth of tetragonal $D0_{22}$ - Mn_3 Ge films, as well as their PMA properties. Among these buffer layers, we have firstly introduced the ultra-thin Fe film as the seed layer to induce homoepitaxial growth of Mn_3 Ge films, thus enhance the crystallization and magnetic anisotropy of $D0_{22}$ - Mn_3 Ge films. The film grown on ultra-thin Fe seed layer can obtain a smaller M_S of 116 emu/cm³, largest K_u of 11.4 $Merg/cm^3$, largest squareness of 0.96, lowest surface roughness of 2.38 nm, and single-phase M-H loops compared to those of films grown on other buffer layers. These results make the ultra-thin Fe seed layer as a great candidate for future large thickness-range Mn_3 Ge film fabrication and show extraordinary advantages for using high-PMA-ordered Mn_3 Ge films in spintronics applications.

Declaration of Competing Interest

The authors declare that they have no known competing financial interests or personal relationships that could have appeared to influence the work reported in this paper.

Acknowledgements

The authors acknowledge the support by the National Natural Science Foundation of China (Grant Nos. 11902316, 11972333, 11504327), the Natural Science Foundation of Zhejiang Province (Grant Nos. LQ19F010005, LZ19A020001, LQ15A040002), the National Science Foundation (Grant No. DMR-1905662), the W. M. Keck Foundation, and the Fundamental Research Funds from China Jiliang University.

References

- H.-S.P. Wong, S. Salahuddin, Memory leads the way to better computing, Nat. Nanotechnol. 10 (2015) 191–194.
- [2] T. Newhouse-Illige, Y. Liu, M. Xu, D.R. Hickey, A. Kundu, H. Almasi, C. Bi, X. Wang, J. Freeland, D. Keavney, Voltage-controlled interlayer coupling in perpendicularly magnetized magnetic tunnel junctions, Nat. Commun. 8 (2017) 15232.
- [3] M. Wang, W. Cai, K. Cao, J. Zhou, J. Wrona, S. Peng, H. Yang, J. Wei, W. Kang,

- Y. Zhang, Current-induced magnetization switching in atom-thick tungsten engineered perpendicular magnetic tunnel junctions with large tunnel magnetoresistance, Nat. Commun. 9 (2018) 671.
- [4] S. Yuasa, T. Nagahama, A. Fukushima, Y. Suzuki, K. Ando, Giant room-temperature magnetoresistance in single-crystal Fe/MgO/Fe magnetic tunnel junctions, Nat. Mater. 3 (2004) 868–871.
- [5] J.-G. Zhu, C. Park, Magnetic tunnel junctions, Mater. Today 9 (2006) 36-45.
- [6] H. Yoda, T. Kishi, T. Nagase, M. Yoshikawa, K. Nishiyama, E. Kitagawa, T. Daibou, M. Amano, N. Shimomura, S. Takahashi, High efficient spin transfer torque writing on perpendicular magnetic tunnel junctions for high density MRAMs, Curr. Appl. Phys. 10 (2010) e87–e89.
- [7] S. Ikeda, K. Miura, H. Yamamoto, K. Mizunuma, H. Gan, M. Endo, S. Kanai, J. Hayakawa, F. Matsukura, H. Ohno, A perpendicular-anisotropy CoFeB-MgO magnetic tunnel junction, Nat. Mater. 9 (2010) 721–724.
- [8] J.W. Koo, S. Mitani, T.T. Sasaki, H. Sukegawa, Z.C. Wen, T. Ohkubo, T. Niizeki, K. Inomata, K. Hono, Large perpendicular magnetic anisotropy at Fe/MgO interface, Appl. Phys. Lett. 103 (2013) 4.
- [9] Q.Y. Xiang, R. Mandal, H. Sukegawa, Y.K. Takahashi, S. Mitani, Large perpendicular magnetic anisotropy in epitaxial Fe/MgAl₂O₄(001) heterostructures, Appl. Phys. Express 11 (2018) 5.
- [10] G. Kim, Y. Sakuraba, M. Oogane, Y. Ando, T. Miyazaki, Tunneling magnetoresistance of magnetic tunnel junctions using perpendicular magnetization L₁₀-CoPt electrodes, Appl. Phys. Lett. 92 (2008) 172502.
- [11] J. Jeong, Y. Ferrante, S.V. Faleev, M.G. Samant, C. Felser, S.S. Parkin, Termination layer compensated tunnelling magnetoresistance in ferrimagnetic Heusler compounds with high perpendicular magnetic anisotropy, Nat. Commun. 7 (2016) 10276.
- [12] H. Kurt, K. Rode, M. Venkatesan, P. Stamenov, J.M.D. Coey, High spin polarization in epitaxial films of ferrimagnetic Mn₃Ga, Phys. Rev. B 83 (2011) 020405.
- [13] M. Li, X. Jiang, M.G. Samant, C. Felser, S.S. Parkin, Strong dependence of the tetragonal Mn_{2.1}Ga thin film crystallization temperature window on seed layer, Appl. Phys. Lett. 103 (2013) 032410.
- [14] B. Balke, G.H. Fecher, J. Winterlik, C. Felser, Mn₃Ga, a compensated ferrimagnet with high Curie temperature and low magnetic moment for spin torque transfer applications, Appl. Phys. Lett. 90 (2007) 152504.
- [15] H. Kurt, K. Rode, M. Venkatesan, P. Stamenov, J. Coey, Mn_{3-x}Ga (0 ≤ x ≤ 1): Multifunctional thin film materials for spintronics and magnetic recording, Phys. Status. Solidi. B 248 (2011) 2338–2344.
- [16] L. Zhu, J. Zhao, Perpendicularly magnetized Mn_xGa films: promising materials for future spintronic devices, magnetic recording and permanent magnets, Appl. Phys. A 111 (2013) 379–387.
- [17] H. Lee, H. Sukegawa, J. Liu, S. Mitani, K. Hono, Perpendicularly magnetized (001)-textured D0₂₂ MnGa films grown on an (Mg_{0.2}Ti_{0.8})O buffer with thermally oxidized

- Si substrates, J. Appl. Phys. 118 (2015) 5.
- [18] H. Lee, H. Sukegawa, S. Mitani, K. Hono, Order parameters and magnetocrystalline anisotropy of off-stoichiometric D0₂₂ Mn_{2.36}Ga epitaxial films grown on MgO (001) and SrTiO₃ (001), J. Appl. Phys. 118 (2015) 7.
- [19] H. Lee, H. Sukegawa, J. Liu, S. Mitani, K. Hono, Tuning the magnetic properties and surface morphology of D0₂₂ Mn₃₋₈Ga films with high perpendicular magnetic anisotropy by N doping, Appl. Phys. Lett. 109 (2016) 4.
- [20] S. Mizukami, A. Sakuma, A. Sugihara, T. Kubota, Y. Kondo, H. Tsuchiura, T. Miyazaki, Tetragonal D0₂₂ Mn_{3+x}Ge epitaxial films grown on MgO (100) with a large perpendicular magnetic anisotropy, Appl. Phys. Express 6 (2013) 123002.
- [21] A. Sugihara, K. Suzuki, T. Miyazaki, S. Mizukami, Magnetic properties of ultrathin tetragonal Heusler D0₂₂-Mn₃Ge perpendicular-magnetized films, J. Appl. Phys. 117 (2015) 17B511.
- [22] A. Sugihara, S. Mizukami, Y. Yamada, K. Koike, T. Miyazaki, High perpendicular magnetic anisotropy in D0₂₂-Mn_{3+x}Ge tetragonal Heusler alloy films, Appl. Phys. Lett. 104 (2014) 132404.
- [23] H. Kurt, N. Baadji, K. Rode, M. Venkatesan, P. Stamenov, S. Sanvito, J. Coey, Magnetic and electronic properties of D0₂₂-Mn₃Ge (001) films, Appl. Phys. Lett. 101 (2012) 132410.
- [24] A. Sugihara, K. Suzuki, S. Mizukami, T. Miyazaki, Structure and magnetic properties of tetragonal Heusler D0₂₂-Mn₃Ge compound epitaxial films with high perpendicular magnetic anisotropy, J. Phys. D: Appl. Phys. 48 (2015) 164009.
- [25] A. Sugihara, K. Suzuki, T. Miyazaki, S. Mizukami, Epitaxial growth of hard ferrimagnetic Mn₃Ge film on rhodium buffer layer, Metals 5 (2015) 910–919.
- [26] J. Coey, New permanent magnets; manganese compounds, J. Phys: Condens. Matter 26 (2014) 064211.
- [27] A. Kobayashi, T. Higo, S. Nakatsuji, Y. Otani, Structural and magnetic properties of Mn_3Ge films with Pt and Ru seed layers, AIP Adv. 10 (2020) 015225.
- [28] N. Awari, S. Kovalev, C. Fowley, K. Rode, R. Gallardo, Y.-C. Lau, D. Betto, N. Thiyagarajah, B. Green, O. Yildirim, Narrow-band tunable terahertz emission from ferrimagnetic Mn_{3-x}Ga thin films, Appl. Phys. Lett. 109 (2016) 032403.
- [29] S. Mizukami, A. Sugihara, S. Iihama, Y. Sasaki, K. Suzuki, T. Miyazaki, Laser-in-duced THz magnetization precession for a tetragonal Heusler-like nearly compensated ferrimagnet, Appl. Phys. Lett. 108 (2016) 012404.
- [30] J. Walowski, M. Münzenberg, Perspective: ultrafast magnetism and THz spintronics, J. Appl. Phys. 120 (2016) 140901.
- [31] D. Betto, Y.-C. Lau, K. Borisov, K. Kummer, N.B. Brookes, P. Stamenov, J.M.D. Coey, K. Rode, Structure, site-specific magnetism, and magnetotransport properties of epitaxial D0₂₂-structure Mn₂Fe_xGa thin films, Phys. Rev. B 96 (2017) 024408.
- [32] J. Balluff, J.-M. Schmalhorst, E. Arenholz, M. Meinert, G. Reiss, Enhancing magnetic properties in Mn₃Ge thin films by doping, Phys. Rev. B 97 (2018) 014403.
- [33] A. Köhler, I. Knez, D. Ebke, C. Felser, S.S.P. Parkin, Loss of anisotropy in strained ultrathin epitaxial L₁₀ Mn-Ga films, Appl. Phys. Lett. 103 (2013) 162406.